Thin Solid Films 693 (2020) 137678

Contents lists available at ScienceDirect

Thin Solid Films

journal homepage: www.elsevier.com/locate/tsf

Photocorrosion of polyaniline-ZnS–ZnO photoelectrode for water splitting

Hyun Kim, Myung-Hoon Oh, Bee Lyong Yang*

School of Materials Science and Engineering, Kumoh National Institute of Technology, 61 Daehak-ro, Gumi-si, Gyeongsangbuk-do 39177, Republic of Korea

ARTICLE INFO

Keywords:
Photocorrosion
Self-oxidation
Microstructural transition
Polyaniline
Zinc sulfide
Zinc oxide

ABSTRACT

Photoelectrodes of polyaniline-coated ZnS film/ZnO nanorods (NRs) for water splitting were evaluated for their photocorrosion behavior. Their microstructure transition and photocatalytic properties were systematically investigated using cyclic voltammetry with light illumination. In photoelectrodes without polyaniline (PANI) coating after 20-cycle tests, photocurrent was reduced by approximately 78%. The ZnO NRs were almost completely photocorroded. On the other hand, PANI-coated photoelectrodes showed no reduction of photocurrent, and no photocorrosion of the ZnS/ZnO structures. Thus, it can be confirmed that the PANI layer has a photocorrosion prevention effect. This effect can be explained by the self-redox potential levels and band alignment of each constituent material relative to the redox potential for water splitting. We report that it is important to prevent the accumulation of photo-excited electrons and holes in photocatalysts. It appears that the PANI-coated ZnS/ZnO structures have sufficient band alignment to prevent this accumulation.

1. Introduction

Photocorrosion can be defined as the phenomenon of self-oxidation or self-reduction with excited holes or electrons in photocatalytic semiconductors, respectively, when they are exposed to solar light. The occurrence of photocorrosion depends on the position of the self-redox potential level of a photocatalytic semiconductor relative to the water-splitting redox potential levels (0 V for H^+/H_2 and 1.23 V for O_2/H_2O vs. NHE @ pH 0). In other words, if the self-oxidation potential level is positioned within the band gap and at the same time at a negative value compared to the water oxidation potential level of 1.23 V O_2/H_2O, excited holes will participate in the self-oxidation reaction rather than in the O_2 evolution reaction ($H_2O_{(l)} + 2h^+ \rightarrow 1/2O_{2(g)} + 2H^+_{(aq)}$) [1–5]. For example, metal chalcogenide compounds such as SnS (E_g = =1.01 eV), PbS (0.37 eV), NiS_2 (0.3 eV), HfS_2 (1.13 eV), FeS_2 (0.95 eV), MnS_2 (0.5 eV), Cu_2S (1.10 eV), and TiS_2 (0.70 eV) can feasibly self-oxidize with holes ($S^{2-}_{(aq)} + 2h^+ \rightarrow S_{(s)}$) [6–10].

One of the methods to prevent photocorrosion is the addition of electron–hole scavengers to the electrolyte, resulting in significant removal of electrons or holes responsible for the photocorrosion reaction. Electron scavengers such as $Na_2S_2O_8$, $AgNO_3$, and $FeCl_3$, and hole scavengers such as methanol, KBr, $Na_2S_2O_3$, Na_2S, and Na_2SO_3, have been reported [11–13]. However, this may be not the ideal solution for photocorrosion, because the consumable additives would need to be supplied constantly. Another way to solve the issue is to deposit films or nanoparticles on the surface of semiconductors sensitive to photocorrosion. This can essentially prevent photocorrosion, resulting from the capture of excited electrons or holes from semiconductors. To make electrons and holes transfer, it is important to adjust the Fermi energy level through proper band alignment between junction semiconductors. This can inhibit the accumulation of excited carriers inside the semiconductors, blocking photocorrosion reactions. For example, it was reported that MoS_2 sheets deposited on CdS/graphene-oxide show a superior prevention effect from photocorrosion [14]. Photo-excited electrons and holes in CdS move to the MoS_2 sheets and the graphene oxide, respectively, so that accumulation of the charge carriers within the CdS does not occur, and photocorrosion reactions are inhibited. Other coated layers on CdS that inhibit photocorrosion include Ni_2P, Polyaniline (PANI), and carbon [15,16]. Electrons photo-excited inside the CdS were extracted and moved to the conduction band of the shell, and the holes reacted with hole scavengers (S^{2-}, SO_3^{2-}) in the electrolyte and were consumed. Photocorrosion reactions were thus inhibited. Similarly, studies on the photocorrosion-inhibiting effects of Ta_3N_5 deposited with co-catalysts such as $Co(OH)_x$ and Co-Pi were reported [17]. The mechanism was the transfer of photo-excited holes in the Ta_3N_5 to the co-catalysts. In the case of Ag_2O decorated with Ag nanoparticles, photo-excited electrons in the Ag_2O were attracted to the Ag, and holes were consumed for the oxidation of dye in the electrolyte [18]. PANI-coated PbS with a core–shell structure was also reported [19]. Photo-excited holes in the PbS reacted chemically with $Na_2S_2O_3$, a hole scavenger, and were involved in the O_2 evolution process. Another way to inhibit photocorrosion is by changing the self-potential level

* Corresponding author.
E-mail address: blyang@kumoh.ac.kr (B.L. Yang).

https://doi.org/10.1016/j.tsf.2019.137678
Received 18 April 2019; Received in revised form 12 September 2019; Accepted 29 October 2019
Available online 31 October 2019
0040-6090/

through alloying. This was observed for alloys of CdS and Mn, $Mn_{1-x}Cd_xS$ ($0 \le x \le 1$) [20]. Furthermore, a method was reported to inhibit photocorrosion by manipulating nano-structures, that is, crystal planes and grain size, with high mobility of electrons and holes [21]. Fast transfer of electrons and holes into the planes or fine grains can cause prevention of photocorrosion due to a lack of electron and hole accumulation in photocatalytic semiconductors. Consequently, if photo-excited electrons and holes, which can cause photocorrosion in photocatalytic semiconductors, are transferred into neighboring layers or consumed in a redox process, then the photocorrosion process can be prevented, essentially by a deficiency of photo-excited electrons and holes in photocatalytic materials.

Although various types of photocorrosion have been reported in many types of materials [22–26], there have been few detailed studies on photocatalytic properties accompanied by nano-structural transitions during the photocorrosion process. In this study, we investigated this transition for nano-scale microstructural and photocatalytic properties depending on the number of cyclic voltammetry tests for PANI-coated ZnS film/ZnO nanorods (NRs). The role of the PANI layer in these samples was systematically examined by a cyclic voltammetry method in which samples were tested for water splitting and compared after 1 cycle and 20 cycles.

2. Experimental details

2.1. Preparation of ZnO NRs on FTO glass

ZnO NRs were grown on a fluorine-doped tin oxide (FTO, ~8 Ω/cm^2, Sigma Aldrich) glass substrate by a hydrothermal method. The substrates were cleaned by ultrasonication in trichloroethylene, acetone, and methanol sequentially for 10 min each and then dried under N_2 blowing. Subsequently, ZnO seed layer was spin-coated on dried FTO glass substrate using ethanolic zinc acetate solution (10 ml ethanol + 30 mM zinc acetate) at 3500 rpm for 30 s. After spin-coating, the seeded FTO substrates were annealed at 350 °C for 30 min in air. The solution for growth of ZnO NRs contained 35 mM zinc nitrate and 35 mM hexamethylenediamine in deionized water. Annealed ZnO seeded substrates were placed against the wall of a glass vial and then maintained at 95 °C for 3 h. As-grown ZnO NRs were cleaned with deionized water and dried under N_2 blowing. Finally, ZnO NRs were crystallized by annealing at 450 °C for 4 h in air [27,28].

2.2. Preparation of ZnS film on ZnO NRs

ZnS film was synthesized on the surface of ZnO NRs by immersing the ZnO NRs/FTO photoelectrode in an aqueous 0.32 M $Na_2S{\bullet}9H_2O$ solution for 12 h. Sulfurization by anion-exchange reaction was carried out in a deionized water bath at 60 °C. $Na_2S{\bullet}9H_2O$ was used as the S^{2-} anion source to form ZnS on the surface of the ZnO NRs, according to the following reaction:

$$ZnO_{(s)} + S^{2-}_{(aq)} + H_2O_{(l)} \rightarrow ZnS_{(s)} + 2OH^-_{(aq)}$$

The photoelectrode was then cleaned with deionized water and absolute ethanol three times and dried at 80 °C for 2 h in a convection oven [29,30].

2.3. Preparation of PANI on ZnS film/ZnO NRs

A PANI layer was electrochemically polymerized on ZnS film/ZnO NRs photoelectrodes using a standard three-electrode configuration, with as-prepared ZnS film/ZnO NRs/FTO as the working electrode, Pt mesh as the counter electrode, and Ag/AgCl/sat.KCl as the reference electrode. Aniline was distilled under low pressure and stored in the dark before use. Electrochemical polymerization of PANI was carried out using cyclic voltammetry at 50 mV/s in 250 ml of 0.5 M aqueous H_2SO_4 [31–33].

2.4. Microstructure characterization

The microstructure of the photoelectrodes was characterized by field-emission scanning electron microscopy using an operating voltage of 10 kV (FE-SEM; 10 kV/JSM-6500 F, JEOL), field-emission transmission electron microscopy (FE-TEM; 200 kV/JEM-2100F HR, JEOL), and X-ray diffraction (XRD, Cu K_α/SWXD, Rigaku) operating in the 2θ scanning mode with Cu-K_α radiation (40 kV, 200 mA) and diffracted beam monochromator, using a step scan mode with the step of 0.02°.

2.5. Photocorrosion and photocatalytic tests

The photocurrent densities of the photoelectrodes for water splitting were measured using a potentiostat (AMT VERSASTAT 3, Princeton Applied Research) with a three-electrode cell comprising Pt mesh as the counter electrode and Ag/AgCl/sat. KCl as the reference electrode separated by a proton exchange membrane in 0.1 M aqueous Na_2SO_4 (pH = 7.15) electrolyte. The photocurrent measurements were followed by cyclic voltammetry tests for photocorrosion investigation using the potentiostat in the voltage range −1.5 to 1.5 V under white light (consisting of UV and visible light) illumination. Using a 1 kW xenon lamp (Newport) with the infrared wavelengths filtered out by water, 1 cm^2 of the working electrode was exposed. The light irradiance, measured using a thermopile detector, was 100 mW/cm^2.

3. Results and discussion

In this study, the photocorrosion properties of ZnS film/ZnO NR heterojunctions with PANI layers for water splitting were investigated. To fabricate the composite, first ZnO NRs were grown on an FTO substrate by a hydrothermal method, then ZnS layers were formed via sulfurization, followed by PANI coating via electroplating. In Fig. 1, SEM images are shown for ZnS film/ZnO NRs and PANI/ZnS film/ZnO NRs after a 1-cycle test in cyclic voltammetry mode. Fig. 1(a) and (b) show representative surface and cross-sectional views of ZnS film/ZnO NRs, in which ZnO NRs with an average length of about 1.5 μm and an

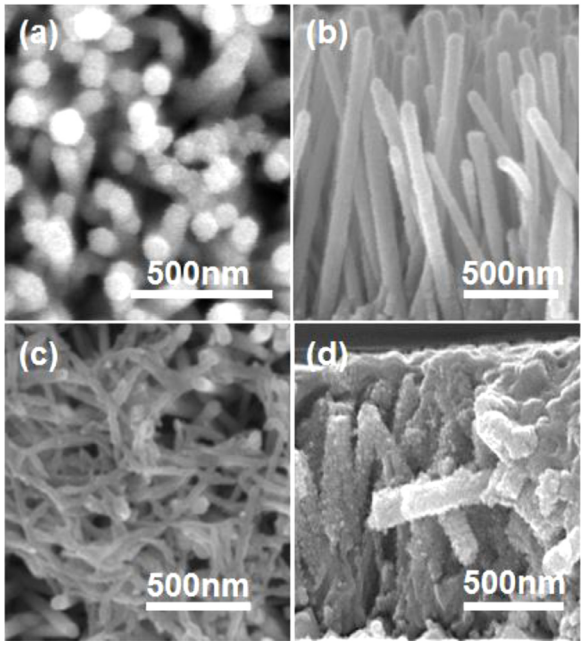

Fig 1. SEM images of ZnS film/ZnO NRs, and PANI/ZnS film/ZnO NRs after 1-cycle test in cyclic voltammetry mode: surface (a and c), and cross-sectional views (b and d).

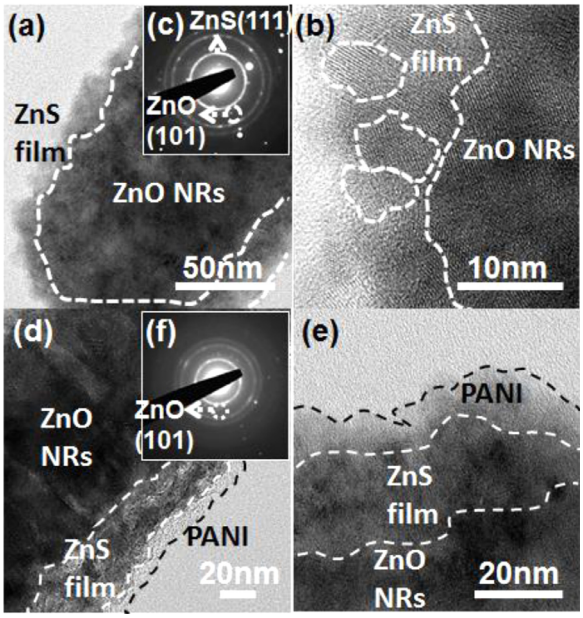

Fig 2. TEM images of ZnS film/ZnO NRs, and PANI/ZnS film/ZnO NRs after 1-cycle test in cyclic voltammetry mode: bright field (a and d), high-resolution lattice fringes (b and e), and selective electron diffraction patterns (c and f).

average width of about 90 nm were grown slantwise and cross-arranged on FTO. The ZnS films are uniformly coated on the surface of the ZnO NRs. In Fig. 1(c) and (d), surface and cross-sectional images of PANI-coated ZnS film/ZnO NRs are shown. It can be seen that the spaces between the ZnS film-coated ZnO NRs are completely filled with PANI. The morphology of electropolymerized PANI is similar to that of glue.

The TEM bright field image and high-resolution lattice-fringes are shown for the ZnS film/ZnO NRs sample after a 1-cycle test in cyclic voltammetry mode in Fig. 2(a) and (b), respectively. The ZnS film consists of densely agglomerated nanoparticles (NPs) with an average diameter of about 7.5 nm. Fig. 2(c) shows the selective electron diffraction patterns from TEM analysis for ZnS film/ZnO NRs. The (101) diffraction spot (zincite, hexagonal, space group P63mc; JCPDS card no. 36-1451) of single-crystalline ZnO NRs and the (111) diffraction ring (sphalerite, cubic, space group F43m; JCPDS card no. 05-0566) of polycrystalline ZnS film are shown. The bright-field TEM image and high-resolution lattice-fringes for PANI/ZnS film/ZnO NRs after a 1-cycle test in the cyclic voltammetry mode are shown in Fig. 2(d) and (e), respectively. The PANI layer of ~10 nm thickness is coated uniformly on the surface of the ZnS-NP film. Fig. 2(f) shows the selective electron diffraction patterns from TEM analysis of the PANI/ZnS film/ZnO NRs. The (101) diffraction spot of single crystalline ZnO NRs and the (111) diffraction ring diffraction of polycrystalline ZnS film are observed.

Photocurrent densities measured after a 1-cycle and a 20-cycle (~1.5 h) test under white light illumination in cyclic voltammetry mode for ZnS film/ZnO NRs and PANI/ZnS film/ZnO NRs are compared in Fig. 3(a) and (b), respectively. Photocurrent densities of the samples for water splitting were measured in a photoelectrochemical cell under white light exposure using infrared (IR) filters. The photocurrent density corresponding to pure photo-response was measured by using a chopping light source (on-off). The measured photocurrent density is the photo-response difference between the on- and off-states of the light source. The photocurrent densities of the ZnS film/ZnO NRs electrode after the 1-cycle and 20-cycle test were ~0.42 and ~0.09 mA/cm^2 at 1 V, respectively. In this measurement, the photocurrent density of the 20-cycle sample was reduced by approximately 78% compared with the 1-cycle sample. It is believed that this significant reduction of photocurrent density is due to photocorrosion with an increasing number of cycles in the voltammetry test. As seen in the inset photo of Fig. 3(a), photocorrosion damage occurs on the electrode. The brown color of the electrode after one cycle becomes transparent after 20 cycles. It is thought that this is due to photocorrosion of the ZnS film and ZnO NRs. Meanwhile, for the PANI/ZnS film/ZnO NRs electrode, the photocurrent densities after one cycle and 20 cycles are ~0.54 and ~0.60 mA/cm^2 at 1 V, respectively, as shown in Fig. 3(b). In this measurement, the photocurrent density of the 20-cycle sample is slightly increased when compared to that of the 1-cycle sample. It is generally increasing by increasing cycle numbers during cyclic voltammetry measurement. It is estimated that increasing activity of refrained electrons–holes at the interfaces improves photocurrent density of the samples. The UPS measurements confirmed the band alignment of PANI/ZnS/ZnO suitable for the effective charge transferring (see Fig. 4). It means photo-excited electrons and holes can effectively separate and transfer at each interface.

We attribute this almost constant photocurrent density to an absence of photocorrosion in PANI-coated ZnS film/ZnO NRs during the cyclic voltammetry test. As seen in the inset photo in Fig. 3(b), no photocorrosion of the electrode is evident. The color of the electrode after one cycle is almost unchanged after 20 cycles. We believe this is due to a photocorrosion prevention effect of the PANI coating on the ZnS film/ZnO NRs sample.

X-ray diffraction patterns for ZnS film/ZnO NRs and PANI/ZnS film/ZnO NRs after one cycle and 20 cycles in cyclic voltammetry mode, respectively, are compared in Fig. 5. In the X-ray diffraction pattern of the ZnS film/ZnO NRs electrode after the 20-cycle test, peaks for ZnO crystal planes such as (002), (101), (102), (110), and (103) have completely disappeared, and peaks for ZnO (100) and ZnS (111) planes have significantly decreased, when compared to the pattern for the 1-cycle tested sample (see Fig. 5(a)). On the other hand, in the X-ray diffraction pattern of the PANI-coated ZnS film/ZnO NRs electrode after the 20-cycle test, all peaks for ZnO and ZnS crystal planes are completely preserved, when compared to the pattern from the 1-cycle tested sample (see Fig. 5(b)). This is in agreement with the results of the photocurrent measurements discussed in Fig. 3. We believe that the presence of the PANI layer is the main contributor to the inhibition of photocorrosion.

Changes in microstructure accompanying the cyclic voltammetry tests under white light illumination were investigated by SEM and TEM. SEM images for surface and cross-sectional views of the ZnS film/ZnO NRs sample after the 20-cycle test in cyclic voltammetry mode are shown in Fig. 6(a) and (b), respectively. Dissolution of the ZnS film/ZnO NRs is observed. The ZnS is partly photocorroded and its hollow structures are observed, whereas the ZnO NRs are completely dissolved and aggregated with each other. This SEM observation corresponds to the results of XRD measurements, in which several ZnO peaks disappeared and the peak intensities of some ZnS and ZnO planes decreased. We attribute this to photocorrosion in the central part of the NRs, compared to the 1-cycle tested samples of Fig. 1(a) and (b).

SEM images for surface and cross-sectional views of the PANI-coated ZnS film/ZnO NRs sample after the 20-cycle test in cyclic voltammetry mode under light illumination are shown in Fig. 6(c) and (d), respectively. The PANI-coated ZnS film/ZnO NRs are preserved without dissolution, compared to the 1-cycle tested samples of Fig. 1(c) and (d). This SEM observation corresponds to the results of X-ray diffraction measurements in which the intensities of the ZnO and ZnS peaks were preserved. Again, this can be attributed to the inhibition of photocorrosion by the PANI layer, compared to the 20-cycle tested samples of Fig. 6(a) and (b), in which the samples without the PANI layer show significant photocorrosion.

Bright-field TEM images and the high-resolution lattice-fringes for the ZnS film/ZnO NRs sample after 20 cycles in the cyclic voltammetry mode under light illumination are shown in Fig. 7(a) and (b), respectively. The ZnO NRs are significantly photocorroded and partially vacant. The ZnS film are also partially decomposed. Finally, a partially

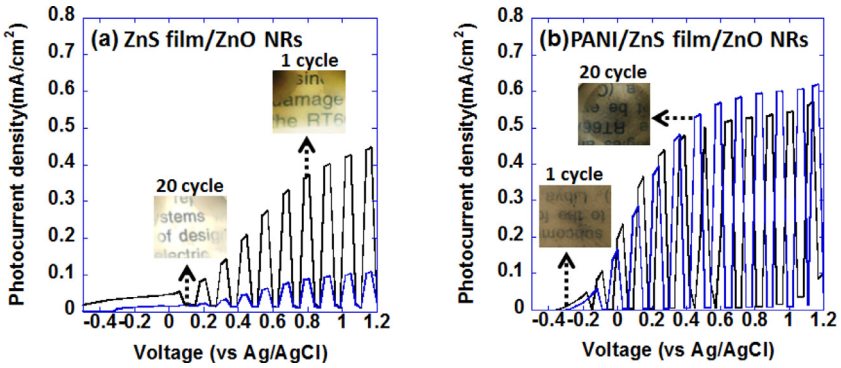

Fig 3. Photocurrent density measured after 1-cycle and 20-cycle test in cyclic voltammetry mode of (a) ZnS film/ZnO NRs, and (b) PANI/ZnS film/ZnO NRs.

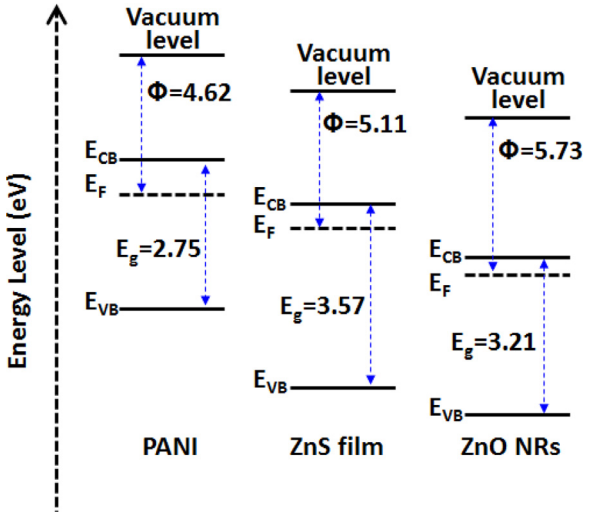

Fig 4. Band alignment based on UPS measurement of the PANI/ZnS film/ZnO NRs.

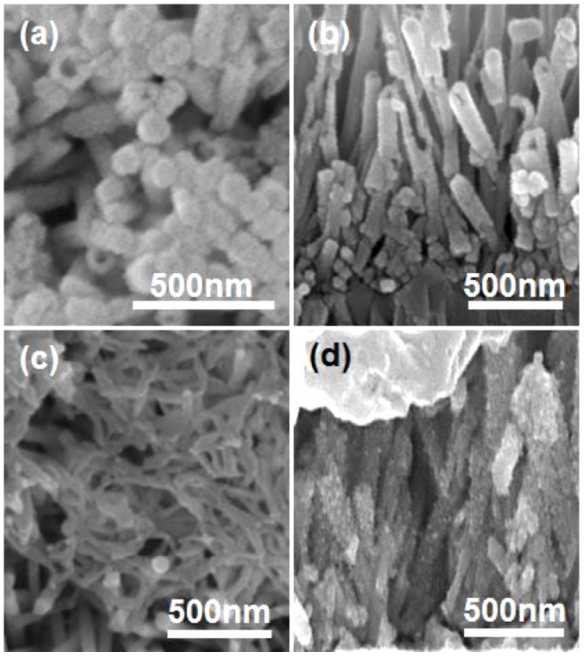

Fig 6. SEM images of ZnS film/ZnO NRs, and PANI/ZnS film/ZnO NRs after 20-cycle test in cyclic voltammetry mode: surface (a and c), and cross-sectional views (b and d).

corroded ZnS-shell structure with a vacant ZnO-NRs-core is observed. Fig. 7(c) shows the selective electron diffraction patterns from TEM for the ZnS film/ZnO NRs after the 20-cycle test. The (101) diffraction spot of single-crystalline ZnO NRs is not observed. A ring shape consisting of many (111) diffraction dots from polycrystalline ZnS film is observed, and can be compared to the sample after one cycle, in which the complete ring-line of the (111) diffraction from polycrystalline ZnS film is observed. The difference between these two patterns is attributed to partial dissolution of the ZnS film. Bright-field TEM images and high-resolution lattice-fringes for PANI-coated ZnS film/ZnO NRs after the 20-cycle test in the cyclic voltammetry mode under light illumination are shown in Fig. 7(d) and (e), respectively. The PANI-coated electrode is not photocorroded after 20 cycles. Fig. 7(f) shows the selective electron diffraction pattern by TEM for PANI/ZnS film/ZnO NRs after the 20-cycle test. The (101) diffraction spot of single-crystalline ZnO NRs and the (111) diffraction ring diffraction of polycrystalline ZnS film

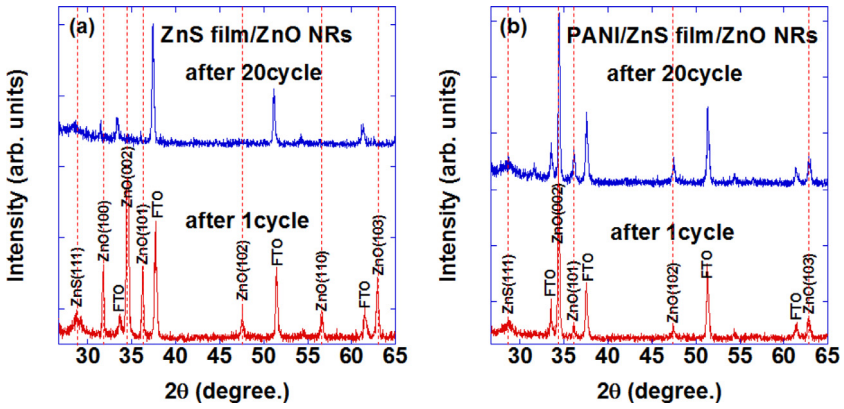

Fig 5. X-ray diffraction patterns of (a) ZnS film/ZnO NRs and (b) PANI/ZnS film/ZnO NRs after 1-cycle and 20-cycle test in cyclic voltammetry mode.

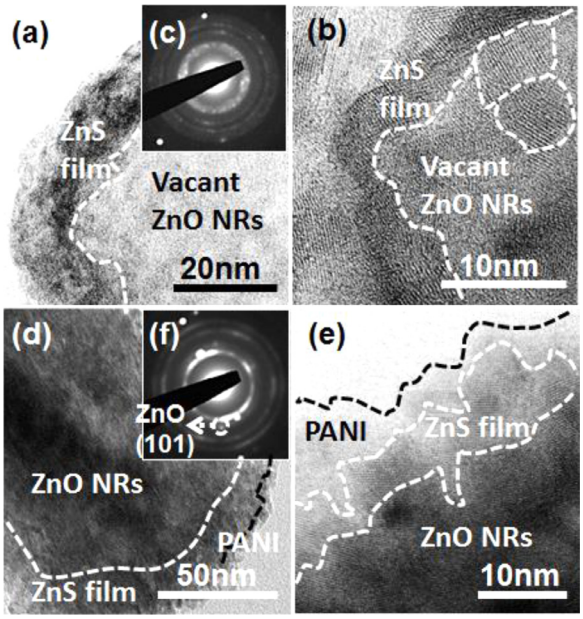

Fig 7. TEM images of ZnS film/ZnO NRs, and PANI/ZnS film/ZnO NRs after 20-cycle test in cyclic voltammetry mode: bright field (a and d), high-resolution lattice fringes (b and e), and selective electron diffraction patterns (c and f).

are identical to those from the sample after one cycle.

The detailed mechanism can be described by the schematic diagram shown in Fig. 8, based on UPS(ultraviolet photoelectron spectroscopy) measurement results(see Fig. 4). Fig. 8(a) shows a schematic electron–hole transfer diagram for the self-oxidation of ZnS film/ZnO NRs, and Fig. 8(b) depicts the self-oxidation inhibition of ZnS film/ZnO NRs by the PANI layer. If the self-oxidation potential level (for example, for ZnO, 0.9 V vs. NHE, pH 0) of a photocatalyst is located at an energy site within the band gap and is simultaneously more negative than the potential level of 1.23 V (vs. NHE, pH 0) for the O_2/H_2O oxidation reaction, the participation of photo-excited holes in the self-oxidation reaction (for example, $ZnO_{(s)} + 2h^+ \rightarrow Zn^{2+}_{(aq)} + 1/2O_{2(g)}$) is more thermodynamically stable than the O_2 evolution reaction ($H_2O_{(l)} + 2h^+ \rightarrow 1/2O_{2(g)} + 2H^+_{(aq)}$). Thus, as shown in Fig. 8(a), the holes accumulated inside ZnO can decompose it. Similarly, the self-oxidation potential level (0.35 V vs. NHE, pH 0) of ZnS is located at an energy site within the band gap which is more negative than the potential level of 1.23 V (vs. NHE, pH 0) for the O_2/H_2O oxidation reaction. Thus, the participation of photo-excited holes in the self-oxidation reaction ($ZnS_{(s)} + 2h^+ \rightarrow Zn^{2+}_{(aq)} + S_{(s)}$) is more thermodynamically stable than the O_2 evolution reaction ($H_2O_{(l)} + 2h^+ \rightarrow 1/2O_{2(g)} + 2H^+_{(aq)}$). Photocorrosion of ZnS will be dominant because the self-redox potential of ZnS is more negative than that of ZnO from a thermodynamic point of view. As shown in Fig. 8(a), the holes accumulated inside ZnS can decompose this compound. However, as can be inferred from the SEM and TEM images (Fig. 6(b), and 7(a), respectively), ZnO NRs were almost completely photocorroded, but the ZnS film was only partially photo-decomposed. The reason for this difference is that the hole scavenger Na_2SO_4 was used as an additive in the electrolyte for the cyclic voltammetry test, and can consume holes near the ZnS rather than near the ZnO NRs. More holes accumulate in ZnO NRs than in the ZnS; consequently, ZnS shows partial photocorrosion behavior compared to the almost complete photocorrosion of ZnO. As shown in Fig. 8(b), the PANI coating can contribute to the inhibition of photocorrosion in ZnS/ZnO structures. The reason for this is that excited holes in ZnS/ZnO can easily transfer into the PANI layer, due to the more negative potential level of PANI, and the accumulation of excited holes within the ZnS/ZnO can be completely prevented. XPS measurement results confirmed the compositions of PANI/ZnS film/ZnO NRs (see Fig. 9) and no interaction between PANI layer and ZnS film/ZnO NRs. That is, accumulation of excess photo-induced holes at surface of ZnS/ZnO causes the photocorrosion.

Thus, it is prevented if those holes were transferred from the surface of ZnS/ZnO and accumulated on the surface of PANI [34]. The holes transferring is highly significant because the measurement results in Fig. 4 showed suitable band alignment (see also the discussion in Fig. 8). Thus, the PANI-coated ZnS/ZnO showed superior behavior with respect to photocorrosion. Various candidates for photocorrosion prevention such as NiO, RuO_2 and carbon nanotubes have been reported [35–37]. However we believe that PANI is a superior photocorrosion protection layer for ZnS/ZnO because of dense formation of PANI on

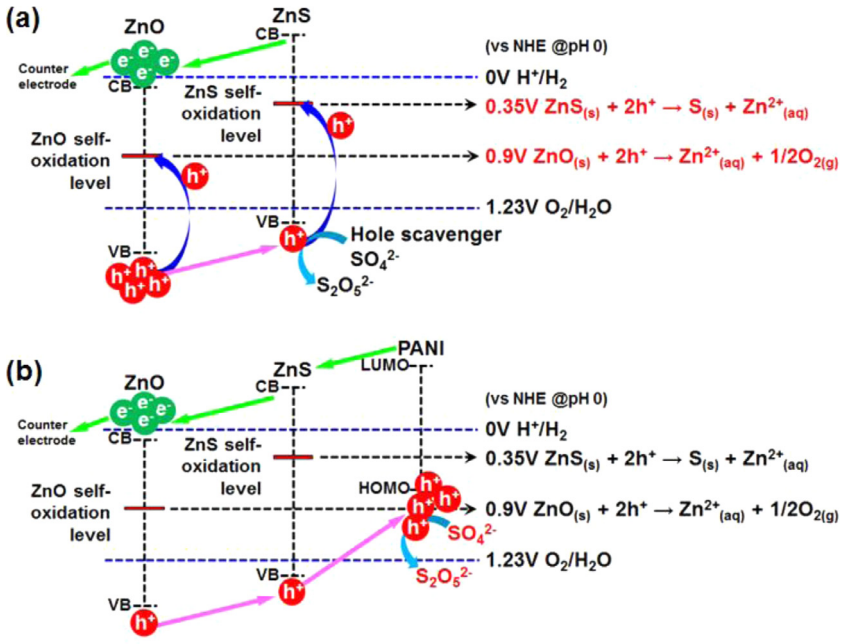

Fig 8. Electron–hole transfer schematics, based on UPS measurement, of (a) ZnS film/ZnO NRs self-oxidation, and (b) self-oxidation inhibition of ZnS film/ZnO NRs by PANI layer, related to water redox potential.

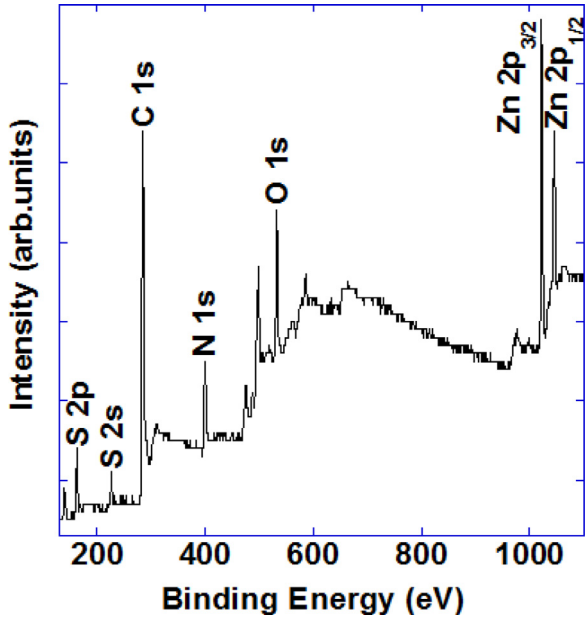

Fig 9. X-ray photoelectron spectroscopy (XPS) spectra of the PANI/ZnS/ZnO.

ZnS film/ZnO NRs and suitable band alignment to avoid accumulation of holes at the interface.

In summary, PANI-coated ZnS film/ZnO NR photoelectrodes were fabricated and evaluated for their photocorrosion performance. The role of the PANI layer, which leads to superior photocorrosion performance, can be understood in terms of self-oxidation potential levels and band alignment of each constituent material relative to the water redox potential.

4. Conclusions

In this study, photoelectrodes of PANI-coated ZnS film/ZnO NRs were investigated for their photocorrosion behavior during water splitting. Their microstructure transition and photocatalytic properties were systematically evaluated using cyclic voltammetry tests with light illumination. To fabricate the PANI-coated ZnS film/ZnO NRs samples, ZnS film was coated on the surface of ZnO NRs which were synthesized by a hydrothermal technique, and then a PANI layer was coated on the ZnS film/ZnO NRs. After these photoelectrode samples were tested as a function of the number of voltammetry cycles under light illumination, changes in the photocurrent and microstructure were compared for 1- and 20-cycle tests by photo-response measurements, SEM, TEM, and XRD. In the photoelectrodes without PANI layers after the 20-cycle tests, photocurrents were reduced by approximately 78%. ZnO NRs were almost completely photocorroded, while ZnS films were partially decomposed with a hollow structure. On the other hand, PANI-coated photoelectrodes showed no reduction of photocurrent and no photocorrosion in the ZnS/ZnO structures. Thus, it was confirmed by this study that the PANI layer in these photoelectrodes has a photocorrosion prevention effect. The effect can be explained by the self-redox potential levels and band alignment of each constituent material relative to the water redox potential for water splitting. Based on these results, it is important to prevent the accumulation of photo-excited electrons and holes in photocatalysts. It appears that PANI-coated ZnS/ZnO structures have sufficient band alignment to prevent photocorrosion.

Acknowledgments

None.

Funding

This work was supported by the Basic Science Research Program through the National Research Foundation of Korea (NRF) funded by the Ministry of Education, Science, and Technology (MEST) [grant number 2017R1D1A1B03034141].

References

[1] S. Chen, L.W. Wang, Thermodynamic oxidation and reduction potentials of photocatalytic semiconductors in aqueous solution, Chem. Mater. 24 (2012) 3659–3666 http://doi.org/10.1021/cm302533s.
[2] L.J. Guo, J.W. Luo, T. He, S.H. Wei, S.S. Li, Photocorrosion-Limited maximum efficiency of solar photoelectrochemical water splitting, Phys. Rev. Appl. 10 (2018) 064059–064077 http://doi.org/10.1103/PhysRevApplied.10.064059.
[3] A. Olivo, E. Ghedini, M. Signoretto, M. Compagnoni, L. Rossetti, Liquid vs. gas phase co photoreduction process: which is the effect of the reaction medium? Energies 10 (2017) 1394–1407 https://doi.org/10.3390/en10091394.
[4] D.R. Baker, C.A. Lundgren, Electrochemical determination of the galliumnitride photocorrosion potential in acidic media, J. Mater. Chem. A 5 (2017) 20978–20984 https://doi.org/10.1039/C7TA04545J.
[5] J.H. Kim, J.S. Lee, $BiVO_4$-Based heterostructured photocatalysts for solar water splitting: a review, Energy Environ. Focus 3 (2014) 339–353 https://doi.org/10.1166/eef.2014.1121.
[6] H.I. Stawska, M.A. Popenda, E.B. Pawlik, Combining hollow core photonic crystal fibers with multimode, solid core fiber couplers through arc fusion splicing for the miniaturization of nonlinear spectroscopy sensing devices, Fibers 6 (2018) 77–92 https://doi.org/10.3390/fib6040077.
[7] A. Kagkoura, T. Skaltsas, N. Tagmatarchis, Transition-Metal chalcogenide/graphene ensembles for light-induced energy applications, Chem. Curr. J. 23 (2017) 12967–12979 https://doi.org/10.1002/chem.201700242.
[8] O. Stroyuk, A. Raevskaya, N. Gaponik, Solar light harvesting with multinary metal chalcogenide nanocrystals, Chem. Soc. Rev. 47 (2018) 5354–5422 https://doi.org/10.1039/C8CS00029H.
[9] R.K.M. Raghupathy, H. Wiebeler, T.D. Kühne, C. Felser, H. Mirhosseini, Database screening of ternary chalcogenides for P-type transparent conductors, Chem. Mater. 30 (2018) 6794–6800 https://doi.org/10.1021/acs.chemmater.8b02719.
[10] H.Q. Fu, L. Zhang, C.W. Wang, L.R. Zheng, P.F. Liu, H.G. Yang, 1D/1D Hierarchical nickel sulfide/phosphide nanostructures for electrocatalytic water oxidation, ACS Energy Lett. 3 (2018) 2021–2029 https://doi.org/10.1021/acsenergylett.8b00982.
[11] C. Li, H. Wang, S.B. Naghadeh, J.Z. Zhang, P. Fang, Visible light driven hydrogen evolution by photocatalytic reforming of lignin and lactic acid using one-dimensional nis/cds nanostructures, Appl. Catal. B Environ. 227 (2018) 229–239. https://doi.org/10.1016/j.apcatb.2018.01.038.
[12] M. Lamers, S. Fiechter, D. Friedrich, F.F. Abdi, R.V.D. Krol, Formation and suppression of defects during heat treatment of $BiVO_4$ photoanodes for solar water splitting, J. Mater. Chem. A 6 (2018) 18694–18700 https://doi.org/10.1039/C8TA06269B.
[13] L. Shi, S. Zhuo, M. Abulikemu, G. Mettela, T. Palaniselvam, S. Rasul, B. Tang, B. Yan, N.B. Saleh, P. Wang, Annealing temperature effects on photoelectrochemical performance of bismuth vanadate thin film photoelectrodes, RSC Adv. 8 (2018) 29179–29188 https://doi.org/10.1039/C8RA04887H.
[14] M.Q. Yang, C. Han, Y.J. Xu, Insight into the effect of highly dispersed mos_2 versus layer-structured MoS_2 on the photocorrosion and photoactivity of CDS in graphene − CDS − MoS_2 composites, J. Phys. Chem. C 119 (2015) 27234–27246 https://doi.org/10.1021/acs.jpcc.5b08016.
[15] W. Zhen, X. Ning, B. Yang, Y. Wu, Z. Li, G. Lu, The enhancement of CDS photocatalytic activity for water splitting via anti-photocorrosion by coating Ni_2P shell and removing nascent formed oxygen with artificial gill, Appl. Catal. B Environ. 221 (2018) 243–257 https://doi.org/10.1016/j.apcatb.2017.09.024.
[16] Y. Hu, X. Gao, L. Yu, Y. Wang, J. Ning, S. Xu, X.W. Lou, Carbon-coated CDS petalous nanostructures with enhanced photostability and photocatalytic activity, Angew. Chem. Int. Ed. 52 (2013) 5636–5639 https://doi.org/10.1002/anie.201301709.
[17] K. Xu, A. Chatzitakis, I.J.T. Jensen, M. Grandcolas, T. Norby, $TaN/Co(OH)_x$ composites as photocatalysts for photoelectrochemical water splitting, Photochem. Photobiol. Sci. 18 (2019) 837–844 https://doi.org/10.1039/C8PP00312B.
[18] H. Xu, J. Xie, W. Jia, G. Wu. Y. Cao, The formation of visible light-driven Ag/Ag_2O photocatalyst with excellent property of photocatalytic activity and photocorrosion inhibition, J. Colloid Interface Sci. 516 (2018) 511–521 https://doi.org/10.1016/j.jcis.2018.01.071.
[19] M. Rabia, H.S.H. Mohamed, M. Shaban, S. Taha, Preparation of polyaniline/PbS core–shell nano/microcomposite and its application for photocatalytic H_2 electrogeneration from H_2O, Sci. Rep. 8 (2018) 1107–1117 https://doi.org/10.1038/s41598-018-19326-w.
[20] K. Ikeue, S. Shiiba, M. Machida, Novel visible-light-driven photocatalyst based on Mn-Cd-S for efficient H_2 evolution, Chem. Mater. 22 (2010) 743–745 https://doi.org/10.1021/cm9026013.
[21] C.Y. Toe, J. Scott, R. Amal, Y.H. Ng, Recent advances in suppressing the photocorrosion of cuprous oxide for photocatalytic and photoelectrochemical energy conversion, J. Photochem. Photobiol. C (2018), https://doi.org/10.1016/j.jphotochemrev.2018.10.001.
[22] Y.C. Liang, C.C. Wang, Surface crystal feature-dependent photoactivity of ZnO–ZnS composite rods via hydrothermal sulfidation, RSC Adv. 8 (2018) 5063–5070

https://doi.org/10.1039/C7RA13061A.
[23] S.B.A. Hamid, S.J. Teh, C.W. Lai, Photocatalytic water oxidation on ZnO:a review, Catalysts 7 (2017) 93–106 https://doi.org/10.3390/catal7030093.
[24] C. Wang, L. Wang, J. Jin, J. Liu, Y. Li, M. Wu, L. Chen, B. Wang, X. Yang, B.L. Su, Probing effective photocorrosion inhibition and highly improved photocatalytic hydrogen production on monodisperse PANI@CdS core–shell nanospheres, Appl. Catal. B Environ. 188 (2016) 351–359 https://doi.org/10.1016/j.apcatb.2016.02.017.
[25] H. Zhang, R. Zong, Y. Zhu, Photocorrosion inhibition and photoactivity enhancement for zinc oxide via hybridization with monolayer polyaniline, J. Phys. Chem. C 113 (2009) 4605–4611 https://doi.org/10.1021/jp810748u.
[26] V. Gilja, I. Vrban, V. Mandić, M. Žic, Z.H. Murgić, Preparation of a PANI/ZnO composite for efficient photocatalytic degradation of acid blue, Polymers 10 (2018) 940–956 https://doi.org/10.3390/polym10090940.
[27] M. Brzezińska, P.G. Muñoz, A.M. Ruppert, N. Keller, Photoactive ZnO materials for solar light induced Cu_xO–ZnO catalyst preparation, Materials 11 (2018) 2260–2279 https://doi.org/10.3390/ma11112260.
[28] F. Wang, Y. Zhou, X. Pan, B. Lu, J. Huang, Z. Ye, Enhanced photocatalytic properties of ZnO nanorods by electrostatic self-assembly with reduced graphene oxide, Phys. Chem. Chem. Phys. 20 (2018) 6959–6969 https://doi.org/10.1039/C7CP06909J.
[29] C.H. Kao, W.M. Su, C.Y. Li, W.C. Weng, C.Y. Weng, C.C. Cheng, Y.S. Lin, C.F. Lin, H. Chen, Fabrication and characterization of ZnS/ZnO core shell nanostructures on silver wires, AIP Adv. 8 (2018) 065106-06513 https://doi.org/10.1063/1.5027015.
[30] N. Abbas, K.T. Rasoul, Z.J. Shanan, New method of preparation ZnS nano size at low pH, Int. J. Electrochem. Sci. 8 (2013) 3049–3056.
[31] S.H. Mujawar, S.B. Ambade, T. Battumur, R.B. Ambade, S.H. Lee, Electropolymerization of polyaniline on titanium oxide nanotubes for supercapacitor application, Electrochim. Acta 56 (2011) 4462–4466. https://doi.org/10.1016/j.electacta.2011.02.043.
[32] C. Dalmolin, S.C. Canobre, S.R. Biaggio, R.C.R. Filho, N. Bocchi, Electropolymerization of polyaniline on high surface area carbon substrates, J. Electroanal. Chem. 578 (2005) 9–15 https://doi.org/10.1016/j.jelechem.2004.12.011.
[33] Y. Wu, J. Wang, B. Ou, S. Zhao, Z. Wang, S. Wang, Electrochemical preparation of polyaniline nanowires with the used electrolyte solution treated with the extraction process and their electrochemical performance, Nanomaterials 8 (2018) 103–115 https://doi.org/10.3390/nano8020103.
[34] B. Weng, M.Y. Qi, C. Han, Z.R. Tang, Y.J. Xu, Photocorrosion inhibition of semiconductor-based photocatalysts: basic principle, current development, and future perspective, ACS Catal. 9 (2019) 4642–4687 https://doi.org/10.1021/acscatal.9b00313.
[35] Z. Zhang, C. Shao, X. Li, C. Wang, M. Zhang, Y. Liu, Electrospun nanofibers of p-Type NiO/N-type zno heterojunctions photocatalytic activity, ACS Appl. Mater. Interfaces 2 (2010) 2915–2953 https://doi.org/10.1021/am100618h.
[36] K. Kalyanasundaram, K. Borgarello, E. Duonghong, D. Grätzel, Cleavage of water by visible-light irradiation of colloidal CDS solutions; inhibition of photocorrosion by RuO_2, Angew. Chem. Int. Ed. Engl. 20 (1981) 987–988 https://doi.org/10.1002/anie.198109871.
[37] X. Cui, Y. Wang, G. Jiang, Z. Zhao, C. Xu, A. Duan, J. Liu, Y. Wei, W. Bai, The encapsulation of CDS in carbon nanotubes for stable and efficient photocatalysis, J. Mater. Chem. A 2 (2014) 20939–20946 https://doi.org/10.1039/C4TA04549A.